High-Affinity Cation Binding to Organic Cation Transporter 1 Induces Movement of Helix 11 and Blocks Transport after Mutations in a Modeled Interaction Domain between Two Helices

Dmitry Gorbunov, Valentin Gorboulev, Natalia Shatskaya, Thomas Mueller, Ernst Bamberg, Thomas Friedrich, and Hermann Koepsell

Institutes of Anatomy and Cell Biology (D.G., V.G., N.S., H.K.) and Physiological Chemistry (T.M.), University Würzburg, Würzburg, Germany; Department of Biophysical Chemistry, Max-Planck-Institute of Biophysics, Frankfurt, Germany (E.B.); and Institute of Chemistry, Technical University of Berlin, Berlin, Germany (T.F.)

ABSTRACT

Voltage-clamp fluorometry was performed with a cysteine-deprived mutant of rat organic cation transporter 1 (rOCT1) in which Phe483 in transmembrane α-helix (TMH) 11 close to the extracellular surface was replaced by cysteine and labeled with tetramethylrhodamine-6-maleimide. Potential-dependent fluorescence changes were observed that were sensitive to presence of substrates choline, tetraethylammonium (TEA), and 1-methyl-4-phenylpyridinium (MPP) and of the nontransported inhibitor tetrabutylammonium (TBuA). Using potential-dependent fluorescence changes as readout, one high-affinity binding site per substrate and two high-affinity binding sites for TBuA were identified in addition to the previously described single interaction sites. In a structure model of rOCT1 with an inward open cleft that was derived from a known crystal structure of lacY permease, Phe483 is close to Trp147 in TMH 2. In contrast, in a model with an outward open cleft these amino acids are far apart. After replacement of Phe483 or Trp147 by cysteine or serine, high-affinity binding of TBuA leads to inhibition of MPP or TEA uptake, whereas it has no effect on cation uptake by wild-type rOCT1. Coexisting high-affinity cation binding sites in organic cation transporters may collect low concentration xenobiotics and drugs; however, translocation including transitions between outward- and inward-oriented conformations may only be induced when a low-affinity cation binding site is loaded. We propose that cations bound to high-affinity sites may be translocated together with cations bound to low-affinity sites or that they may block the translocation mechanism.

Polyspecific organic cation and carnitine transporters of the *SLC22* transporter family play a pivotal role in the elimination and distribution of cationic drugs, toxins, and metabolic compounds in humans (Koepsell et al., 2003, 2007). The *SLC22* family is a member of the major facilitator superfamily MFS (Pao et al., 1998). It contains facilitative diffusion transporters for organic cations (OCTs), organic anion antiporters, and Na$^+$/carnitine-cotransporters that also operate as Na$^+$-independent cation transporters (OCTNs). The transporters of the *SLC22* family contain 12 potential transmembrane α-helices (TMHs), a large extracellular loop with glycosylation sites, and a large intracellular loop with phosphorylation sites. All these transporters are polyspecific by accepting a variety of compounds with different chemical structures with molecular masses up to 400 Da as substrates, and they are blocked by compounds that may have a larger mass. The biomedical importance of the polyspecific transporters of the *SLC22* family is hallmarked by three findings. First, primary systemic carnitine deficiency is due to loss-of-function mutations of the carnitine transporter OCTN2 (Nezu et al., 1999; Wang et al., 1999). Second, autoimmune diseases such as Crohn's disease, rheumatoid arthritis, and ulcerative colitis are associated with mutations in the transporters OCTN1 and OCTN2 (Tokuhiro et al., 2003; Peltekova

ABBREVIATIONS: OCT, organic cation transporter; OCTN, new organic cation transporter; TMH, transmembrane α-helix; r, rat; TBuA, tetrabutylammonium; TEA, tetraethylammonium; TMRM, tetramethylrhodamine-6-maleimide; MPP, 1-methyl-4-phenylpyridinium; I_m, membrane current; C_m, membrane capacitance; $\Delta F\psi$, potential dependent fluorescence changes; $I_{0.5}$, half-maximal current; r.m.s.d., root-mean-square deviation; MOPS, 3-(N-morpholino)propanesulfonic acid.

et al., 2004; Palmieri et al., 2006). Third, OCT1 mediates uptake of the antidiabetic drug metformin into the liver, and patients with loss-of-function mutations in OCT1 do not respond to metformin treatment (Reitman and Schadt, 2007).

Since the identification of the first polyspecific transporter of the *SLC22* family (Gründemann et al., 1994), research was focused on identification and characterization of new family members. Many new drug transporters of the *SLC22* family have been identified (Koepsell et al., 2003; Koepsell and Endou, 2004). In many organic cation transporters, substrate specificity and tissue distribution were investigated in some detail, and plasma membrane location in the main organs of expression was clarified. Various recent investigations focused on the regulation of these transporters. However, only a few thorough attempts to elucidate the molecular transport mechanisms were undertaken although an understanding of the molecular mechanisms is of large theoretical interest (Budiman et al., 2000; Wang et al., 2000; Volk et al., 2003; Popp et al., 2005; Schmitt and Koepsell, 2005; Zhang et al., 2005). This would provide a rationale for the development of new drugs and help to predict potential side effects of drugs or functional consequences of mutations. Questions to be answered are as follows: 1) How are individual substrates and inhibitors recognized by polyspecific transporters of the *SLC22* family? 2) What is the requirement for a bound compound to be translocated? 3) Which molecular mechanism causes the translocation of substrates? 4) Which are the differences between facilitated diffusion systems, antiporters, and Na^+-cotransporters of the *SLC22* family? and 5) What are the mechanisms that cause transport inhibition after binding of inhibitors?

Several years ago, we started functional characterization of the facilitative organic cation transporters OCT1/2, including analysis of mutants and testing mechanistic models. These transporters are appropriate model systems for investigation because they translocate electrical charge and thus can be analyzed by electrophysiological methods in addition to cation uptake measurements (Koepsell et al., 2003). Fortunately, the elucidation of the crystal structures of the inward open conformation of the lactose permease from *Escherichia coli* and the glycerol phosphate transporter, which belong to the same superfamily as the OCTs, enabled us to construct a molecular model of rat OCT (rOCT1) (Popp et al., 2005). This model suggests that several amino acids that are critical for the specificity of substrates are located in a binding region within the large inwardly open cleft of rOCT1 (Gorboulev et al., 1999, 2005; Popp et al., 2005). Because inhibition of rOCT2 with nontransported inhibitors revealed different affinities from the extracellular compared with the intracellular side of the plasma membrane (Volk et al., 2003), we postulated that rOCT1 and rOCT2 switch between two conformations during transport, thereby mutually opening the cleft to the extra- or intracellular side.

In the present study, we performed voltage-clamp fluorometry with rOCT1. We were able to detect membrane potential- and cation-dependent movements of a fluorescently labeled cysteine that was inserted instead of Phe483 in the TMH 11. Using this readout for cation interaction, we identified high-affinity substrate and inhibitor binding sites. After replacement of individual amino acids in a proposed contact region between the TMH 2 and 11 predicted by our

structure model of rOCT1, high-affinity inhibition of cation uptake by tetrabutylammonium (TBuA) was observed.

Materials and Methods

Materials. [^{3}H]1-Methyl-4-phenylpyridinium (MPP) (3.1 TBq/mmol) and [^{14}C]tetraethylammonium (TEA) (1.9 TBq/mmol) were obtained from Biotrend (Köln, Germany), and tetramethylrhodamine-6-maleimide (TMRM) was from Invitrogen GmbH (Karlsruhe, Germany). The other chemicals were obtained as described previously (Veyhl et al., 1993).

Site-Directed Mutagenesis and Expression of rOCT1 and rOCT1 Mutants in Oocytes. A mutant of rOCT1 (Gründemann et al., 1994) in which all cysteine residues with the exception of those in the large extracellular loop were replaced [rOCT1(10ΔC): C26A, C155A, C417A, C322S, C358A, C418A, C437S, C451M, C470A, and C474A] was prepared as described previously (Sturm et al., 2007). Point mutations were introduced into rOCT1 or rOCT1(10ΔC) by polymerase chain reaction applying the overlap extension method (Ho et al., 1989). Mutants were cloned into the vector pRSSP (Busch et al., 1996), and polymerase chain reaction-derived parts of the mutant constructs were sequenced.

For injection into *Xenopus laevis* oocytes, m7G(5′)ppp(5′)G-capped cRNAs were prepared using the mMESSAGE mMACHINE kit (Ambion, Huntingdon, UK). The purified plasmids were linearized with MluI, the cRNAs were synthesized using SP6 RNA polymerase, and cRNA concentrations were estimated from ethidium bromide-stained agarose gels using polynucleotide marker as standards (Gründemann and Koepsell, 1994).

Stage V to VI oocytes were obtained by partial ovarectomy, defolliculated with collagenase A (Veyhl et al., 1993), and stored for several hours in Ori buffer [5 mM MOPS-NaOH, pH 7.4, 100 mM NaCl, 2 mM KCl, 2 mM $CaCl_2$, and 1 mM $MgCl_2$] containing 50 mg/l gentamicin. The oocytes were injected with 50 nl of H_2O/oocyte containing 10 ng of cRNA encoding rOCT1 or mutants. For transporter expression, the oocytes were incubated for 2 to 3 days at 16°C in Ori buffer containing 50 mg/l gentamicin.

Fluorescence Labeling. Fluorescence labeling was performed with mutants of rOCT1(10ΔCys) in which individual amino acids were replaced by cysteine. Cysteine-specific fluorescence labeling for epifluorescence measurements was achieved by incubating oocytes expressing these mutants for 5 min at room temperature in Ori buffer containing 5 μM TMRM, followed by extensive washes in dye-free buffer (Geibel et al., 2003). These conditions were optimal to achieve robust labeling and to avoid unspecific dye incorporation. To investigate whether TMRM labeling changes the function of mutant rOCT1(10ΔC-F483C), labeling was performed for 1 to 7 min with 100 μM TMRM.

Two-Electrode Voltage-Clamp Epifluorescence Measurements. Measurements were performed in a perfusion chamber that was mounted on the stage of a fluorescence microscope (Axioskop 2FS; Carl Zeiss, Jena, Germany) equipped with a 40× water immersion objective (Geibel et al., 2003). Membrane currents (I_m) were measured using the two-electrode voltage-clamp amplifier CA-1B from Dagan (Minneapolis, MN). Fluorescence was excited by a 100-W tungsten lamp using excitation filter 535DF50, emission filter 565EFLP, and dichroic mirror 570DRLP (Omega Optical Inc., Brattleboro, VT). Fluorescence was measured with a PIN-020A photodiode (United Detector Technology, San Diego, CA) and amplified by patch-clamp amplifier EPC-05 (HEKA, Lambrecht/Pfalz, Germany). pClamp 8 software from Axon Instruments (Foster City, CA) was used for simultaneous recording of fluorescence and current signals.

The potential dependent fluorescence changes ($\Delta F\psi$) were measured after changing the membrane potential from −50 to −170 mV or to +70 mV. In Fig. 2, d and e, $\Delta F\psi$ was normalized according to the equation $\Delta F\psi = F_{(V)} - F_{(-170mV)}/F_{(-170mV)}$, where $F_{(-170mV)}$ represents the fluorescence measured at −170 mV. To determine effects of

cations on voltage-dependent fluorescence changes (Figs. 3 and 4), measurements were performed in the absence of cations and in the presence of various cation concentrations. Fluorescence was recorded after changing the holding potential from -50 to -150 mV, back to -50 mV, and then to $+50$ mV. In general, signals were averaged over three to five runs. The differences between fluorescence amplitudes measured at the end of the pulse to -150 and to $+50$ mV were determined in the absence of cations (ΔF_0) and in the presence of the respective cation concentration (ΔF_{cat}). The cation-induced fluorescence changes ($\Delta F_{cat} - \Delta F_0$) were normalized to the maximal difference in fluorescence observed at saturating cation concentrations $[\Delta F_{cat(max)} - \Delta F_0]$.

Current and Capacitance Measurements. Parallel measurements of I_m and membrane capacitance (C_m) were performed using an TEC-05X amplifier (NPI Electronic, Tamm, Germany) that was controlled by software PULSE and X-Chart (HEKA) (Schmitt and Koepsell, 2005). C_m was measured using a previously described paired ramps approach (Schmitt and Koepsell, 2002). To measure cation-induced inward currents or cation-induced capacitance changes, the oocytes were superfused for 30 s with Ori buffer containing choline, TEA, or TBuA.

Tracer Uptake Measurements. Oocytes injected with cRNAs, and noninjected control oocytes were incubated for 30 min at room temperature with Ori buffer containing [^{14}C]TEA or [^{3}H]MPP, washed in ice-cold Ori buffer supplemented with 100 μM quinine, and analyzed by liquid scintillation counting (Arndt et al., 2001). Expressed rOCT1-dependent uptake was calculated by subtracting the uptake measured in noninjected control oocytes. To determine concentration-inhibition curves, we measured uptake of [^{14}C]TEA (from a 5 μM solution in Ori) or [^{3}H]MPP uptake (from a 2.5 nM solution in Ori) in the presence of various concentrations of unlabeled TBuA, TEA, or MPP. For each substrate concentration or substrate/inhibitor combination, uptake rates were calculated from 7 to 10 cRNA-injected oocytes and from 7 to 10 noninjected control oocytes.

Modeling of the Outward-Facing Conformation of rOCT1. We previously reported a homology model of the rOCT1 (Popp et al., 2005) based on the crystal structure of *E. coli* LacY permease (PDB structure entry 1PV6) (Abramson et al., 2003b), which represents the inward-facing conformation of the transporter. This model is consistent with mutagenesis experiments in which amino acids were identified that participate in cation binding, and it allowed the prediction of additional residues that may also participate in cation binding or may be important for the structure of the inward-open cleft containing the substrate binding region. To further study the transport mechanism, a model of the outward-facing conformation was needed. To obtain such a structural model the putative rearrangement mechanism for lactose transport of LacY permease as proposed by Abramson et al. (2003a,b) was applied to our theoretical rOCT1 model. The N-terminal six helices (N-terminal domain) and C-terminal six helices (C-terminal domain) were separated, and the C-terminal domain was rotated manually as a rigid body until the open cleft at the inward-facing side was closed by contacts between amino acid side chains located at the N termini of helix 5 and the C-terminal end of helix 8 and between amino acids located at the C-terminal side of helix 2 and N-terminal side of helix 11. This initial model of an outward-facing rOCT1 transporter exhibited only a small number of bad van der Waals contacts, which is surprising considering the crude movements applied to the template. The model was subsequently refined, and bad contacts between side chains were removed by side chain rotamer searches using the software Quanta2005 (Accelrys, Cambridge, UK). For further refinement, all helices were separated from interconnecting loops by breaking a peptide bond at the very N and C termini of the individual helices. The helical structure was then maintained by using a set of strict distance restraints (force constants 250 kcal mol^{-1} Å^{-2}), which mimic the H-bond pattern in the individual helices. The helix packing was subsequently optimized by running alternating protocols of

energy minimization (100 steps Adopted Raphson Newton algorithm; Quanta2005) and short in vacuo molecular dynamic simulations (10 ps at 300 K) using only geometrical energy terms (i.e., no electrostatic term). The "disconnected" loops were kept fixed at this point. After 10 rounds of this packing optimization, the peptide bonds between the transmembrane helices and the interconnecting loops were closed, and the loop structures were refined by a similar protocol but restraining the helices with a strong harmonic positional restraint (force constant 250 kcal mol^{-1} Å^{-2}). The final model of the outward-facing rOCT1 displays good backbone and side chain geometries, with 96% of the residues in the most favored or additionally allowed regions of the Ramachandran plot according to PROCHECK analysis. Only six residues occupy phi/psi backbone torsion angles in disallowed regions; however, these residues are located in loop regions.

Calculation and Statistics. We used the Prism software package, version 4.1 (GraphPad Software Inc., San Diego, CA) to compute descriptive statistical parameters. Mean values $\pm$ S.E. derived from independent experiments are presented. Apparent Michaelis-Menten constant (K_m) values for tracer cation uptake and $K_{0.5}$ values for cation-induced currents were determined by fitting the Michaelis-Menten equation to the data. IC$_{50}$ values for inhibition of tracer cation uptake by nonlabeled cations and $K_{0.5}$ values for TBuA-induced capacitance changes were calculated by fitting the Hill equation to the data. The dissociation constant (K_d) values for the effects of cations on TMRM fluorescence of rOCT1 mutant were determined by fitting equations for one-site inhibition, two-site inhibition, or three-site inhibition to the data. Time constants for potential-dependent fluorescence changes were calculated by fitting the data with the sum of two exponential functions. Two-sided Student's t tests were used to prove statistical significance of differences between two groups, and analysis of variance test with post hoc Tukey comparison was used when more than two different groups were compared. Effects of TMRM labeling were evaluated by paired Student's t test.

Results

Identification of Two Amino Acids in rOCT1 That Were Supposed to Move during Cation Transport. Voltage-clamp fluorometry was used to identify amino acids in rOCT1 that take part in conformational transitions during the translocation of organic cations. We replaced individual amino acids for cysteine residues within a mutant in which all cysteine residues with the exception of those in the large extracellular loop were replaced by alanines, serines, or methionine [rOCT1(10ΔC); Sturm et al., 2007] and labeled them with TMRM. Measurements of [^{14}C]TEA and [^{3}H]MPP uptake in *X. laevis* oocytes expressing wild-type rOCT1 or rOCT1(10ΔC) revealed similar maximal transport velocities (V_{max}) and K_m values (Table 1). In contrast, when oocytes expressing rOCT1(10ΔC) were superfused with TEA or choline under voltage-clamp conditions at -50 mV, 2.4-fold higher maximal currents were observed compared with oocytes expressing wild-type rOCT1 (Table 1). In oocytes expressing rOCT1(10ΔC), the TEA concentration required for half-maximal activation of TEA-induced current [$I_{0.5(TEA)}$] was similar to wild-type rOCT1. However, the choline concentration required for half-maximal current [$I_{0.5(choline)}$] was approximately 5-fold higher. The data indicate that the functional properties of rOCT1 are conserved in rOCT1(10ΔC), with the exception of the affinity for choline and an increase of cation-induced currents. These changes are due to the replacement of Cys451 (Sturm et al., 2007).

Reasoning that TMH 11, which contributes to the substrate binding region, is likely to change its position during

transport, we individually exchanged 13 amino acids within TMH 11 of rOCT1(10ΔC) for cysteines (Fig. 1) to generate test constructs for voltage-clamp fluorometry measurements. Previous experiments have shown that Asp475 is located within the substrate binding region (Gorboulev et al., 1999; Popp et al., 2005). The individual cysteine substitution mutants of the rOCT1(10ΔC) construct were expressed in oocytes and tested for uptake of 9 μM [14C]TEA (Fig. 1). For 10 mutants, TEA uptake rates of at least 60% compared with that of rOCT1(10ΔC) were obtained. Cysteine substitution of Asp475 led to a 98.5% reduction of TEA uptake activity. After replacement of Ser471 by cysteine or Pro482 by cysteine, TEA uptake was reduced by 60 and 67%, respectively.

After having confirmed that oocytes expressing rOCT1-(10ΔC), which were incubated for 5 min with 5 μM TMRM, did not respond with voltage-dependent fluorescence changes in the absence and presence of 10 mM choline (data not shown), we expressed the mutants as depicted in Fig. 1 in oocytes and labeled them with 5 μM TMRM for 5 min at room temperature, followed by extensive washes in dye-free buffer. To detect environmental shifts of the TMRM-labeled amino acids in response to changes of the membrane potential and to choline, we measured currents induced by 10 mM choline at −50 mV and fluorescence changes in absence and presence of 10 mM choline that were induced when the potential was switched from −50 to −150 mV or from −50 to +50 mV. Significant choline-induced currents were observed with all TMRM-labeled cysteine mutants shown in Fig. 1 except for mutant D475C. However, potential jump-dependent fluorescence changes were only observed with the TMRM-labeled mutants rOCT1(10ΔC-F483C) and rOCT1(10ΔC-F486C).

Characterization of Potential-Dependent Fluorescence Changes. rOCT1(10ΔC-F483C) and rOCT1(10ΔC-F486C) were expressed in oocytes, labeled with 5 μM TMRM, washed, and clamped to −50 mV. Figure 2 shows potential-dependent fluorescence changes upon superfusion with Ori buffer, with buffer containing various concentrations of choline, or with buffer containing 100 μM TBuA. With rOCT1(10ΔC-F483C) in the absence of organic cations, fluorescence increased when the membrane potential was varied between −170 to +70 mV without reaching saturation (Fig. 2d). In the presence of choline concentrations from 0.1 to 100 μM, the potential-dependent fluorescence changes were diminished (Fig. 2d). If the

buffer contained 10 mM choline or 100 μM TBuA, we observed very small potential-dependent fluorescence changes with an inverted voltage dependence (Fig. 2d). With TMRM-incubated oocytes expressing rOCT1(10ΔC-F486C), no significant fluorescence changes in response to voltage steps were observed in the absence of organic cations (Fig. 2e). In contrast, in the presence of 10 mM choline the mutant showed small fluorescence changes similar to rOCT1(10ΔC-F483C) (Fig. 2e). The data indicate potential- and cation-dependent fluorescence changes after modification of cysteine residues of rOCT1(10ΔC) in positions 483 or 486.

We investigated the time courses of fluorescence changes by TMRM-labeled rOCT1(10ΔC-F483C) that were induced upon switching the membrane potential from −50 mV to different voltages and back to −50 mV as shown in Fig. 2b. The sum of two exponentials could be fitted to the voltage jump-induced fluorescence changes resulting in fast and slow time constants, which both did not exhibited significant voltage dependence within error limits. The fast time constant ranged between 8 and 19 ms, whereas the slow time constant ranged between 84 and 134 ms. The data indicate that TMRM-labeled Cys483 in rOCT1(10ΔC-F483C) performs rapid, potential-dependent movements.

Cation Transport and Choline-Induced Currents Mediated by rOCT1(10ΔC-F483C) before and after Labeling with TMRM. We compared functional properties of rOCT1(10ΔC-F483C) and rOCT1(10ΔC) and subsequently investigated whether TMRM labeling altered the function of rOCT1(10ΔC-F483C). In oocytes expressing rOCT1(10ΔC-F483C), for TEA uptake a K_m value of 143 ± 27 μM and for TEA-induced inward current at −50 mV an $I_{0.5}$ value of 118 ± 8 μM were determined (Table 1). These values were significantly higher compared with rOCT1(10ΔC) or wild-type rOCT1. In contrast, the K_m values for [3H]MPP uptake by rOCT1(10ΔC-F483C), rOCT1(10ΔC), and wild-type rOCT1 were similar (Table 1). In addition, the half-maximal value for choline-induced inward currents [$I_{0.5(choline)}$] was similar in oocytes expressing rOCT1(10ΔC-F483C) and rOCT1(10ΔC) (Table 1). These data indicate that the exchange of Phe483 to cysteine has some effect on the cation selectivity for transport.

To investigate whether labeling of rOCT1(10ΔC-F483C) by TMRM alters transporter function, we incubated oocytes expressing rOCT1(10ΔC) or rOCT1(10ΔC-F483C) for 1 to 7 min

TABLE 1
Functional characterization of the rOCT1(10ΔC) and rOCT1(10ΔC-F483C) in comparison with rOCT1 wild type

Wild-type rOCT1, rOCT1(10ΔC), or rOCT1(10ΔC-F483C) were expressed in oocytes, and concentration activation curves of [14C]TEA uptake, [3H]MPP uptake, TEA-induced currents at −50 mV, and choline-induced currents at −50 mV were measured using 8 to 10 different substrate concentrations. V_{max}, I_{max}, $I_{0.5}$, and K_m values were determined by fitting the Michaelis-Menten equation to the data of individual experiments. Mean values ± S.E. are presented. The number of experiments is shown in parentheses.

Activity	Wild Type	10ΔC	10ΔC-F483C
[14C]TEA uptake			
V_{max} (pmol · oocyte^{-1} · h^{-1})	503 ± 73 (4)	560 ± 95 (3)	385 ± 68 (4)
K_m (μM)	52 ± 21 (11)	67 ± 8 (3)	143 ± 27 (3)***,†††
[3H]MPP uptake			
V_{max} (pmol · oocyte^{-1} · h^{-1})	122 ± 30 (5)	133 ± 23 (3)	57 ± 9 (4)
K_m (μM)	3.9 ± 1.1 (3)	2.5 ± 1.0 (2)	3.0 ± 0.7 (3)
TEA induced current			
I_{max} (nA)	6.4 ± 2.3 (5)[a]	15.3 ± 1.7 (4)*	9.2 ± 4.1 (3)
$K_{0.5}$ (μM)	30 ± 3 (5)[a]	54 ± 5 (4)	118 ± 8 (3)**,†
Choline-induced current			
I_{max} (nA)	18 ± 13 (46)[a]	43 ± 11 (9)*,[a]	25 ± 3.4 (10)
$K_{0.5}$ (μM)	290 ± 180 (6)[a]	1410 ± 240 (3)***,[a]	1300 ± 160 (10)***

* $P < 0.05$, ** $P < 0.01$, and *** $P < 0.001$ compared with wild-type rOCT1.
† $P < 0.05$, ††† $P < 0.001$ compared with rOCT1(10ΔC).
[a] Data reported previously (Sturm et al., 2007).

with 5 or 100 μM TMRM. The oocytes were washed, clamped to -50 mV, and the inward currents induced by superfusion with 10 mM choline [$I_{\text{max(choline)}}$] were measured. No effects of TMRM labeling on currents induced by 10 mM choline [$I_{\text{max(choline)}}$] were observed in oocytes expressing rOCT1-(10ΔC) (data not shown). Likewise, we also did not observe any significant changes in $I_{\text{max(choline)}}$ when oocytes expressing rOCT1(10ΔC-F483C) were incubated in 5 μM TMRM (data not shown). However, after 1-, 3-, 5-, and 7-min incubation in 100 μM TMRM, $I_{\text{max(choline)}}$ was increased by 38 $\pm$ 8, 54 $\pm$ 11, 60 $\pm$ 13, and 62 $\pm$ 14%, respectively ($n = 3$–6 each; $P < 0.05$ for stimulation). The half-maximal concentration for choline-induced inward currents at -50 mV [$K_{0.5(\text{choline})}$] was not significantly changed when the oocytes were incubated for 5 min in either 5 or 100 μM TMRM (data not shown). The data indicate that under the labeling conditions used for fluorescence measurements, only a part of the expressed rOCT1(10ΔC-F483C) molecules is labeled.

Identification of High- and Low-Affinity Cation Binding Sites by Voltage-Clamp Fluorometry. rOCT1(10ΔC-F483C) was expressed in oocytes, incubated for 5 min with 5 μM TMRM, washed with buffer, and differences in the fluorescence amplitudes measured at $+50$ and -150 mV were determined in the absence of organic cations and in the presence of various concentrations of choline, TEA, MPP, and TBuA. For choline effects on potential-dependent fluorescence changes, two different affinities could be distinguished (Fig. 3a); a high-affinity site with a dissociation constant [$K_{\text{d(high-aff.choline)}}$] of
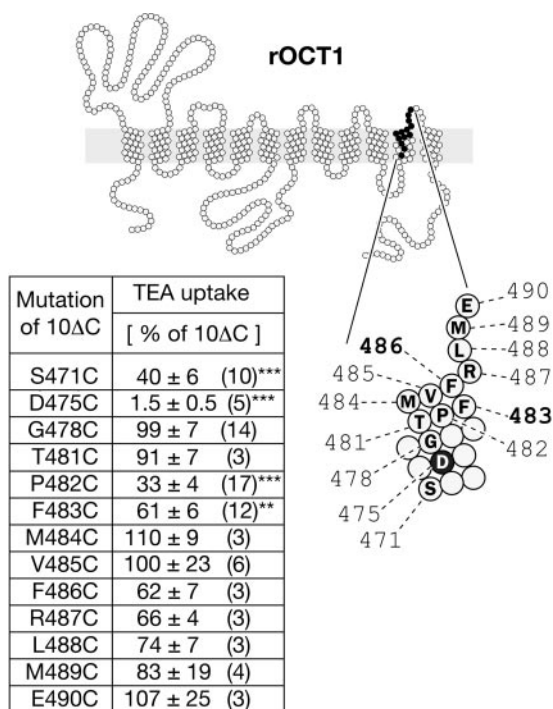

Fig. 1. Location of cysteine mutations in rOCT1(10ΔC) and TEA uptake upon expression in *X. laevis* oocytes. Top, topology model with amino acid residues that were individually replaced by cysteine, indicated by single-letter code. A position that was localized to the cation binding region is highlighted in black. Bottom, relative uptake of 9 μM [^{14}C]TEA in oocytes expressing the indicated cysteine mutants in comparison with oocytes of the same batch expressing rOCT1(10ΔC). Mean values $\pm$ S.E. are indicated. The numbers of independent experiments is given in parentheses. **, $P < 0.01$; ***, $P < 0.001$ for significance of difference between rOCT1(10ΔC) and the respective mutant.

Mutation of 10ΔC	TEA uptake [% of 10ΔC]
S471C	40 ± 6 (10)***
D475C	1.5 ± 0.5 (5)***
G478C	99 ± 7 (14)
T481C	91 ± 7 (3)
P482C	33 ± 4 (17)***
F483C	61 ± 6 (12)**
M484C	110 ± 9 (3)
V485C	100 ± 23 (6)
F486C	62 ± 7 (3)
R487C	66 ± 4 (3)
L488C	74 ± 7 (3)
M489C	83 ± 19 (4)
E490C	107 ± 25 (3)

12 $\pm$ 5 nM and a low-affinity site with a $K_{\text{d(low-aff.choline)}}$ of 0.35 $\pm$ 0.11 mM (the mean values $\pm$ S.E. were calculated from the K_d values determined for individual experiments). It is noteworthy that for rOCT1(10ΔC-F483C), hyperbolic concentration dependencies were observed for choline activation of inward currents at -50 mV after 5-min incubation with 100 μM TMRM (data not shown). These data could well be fitted with a one-site model, resulting in an $I_{0.5(\text{choline})}$ value of 1.8 $\pm$ 0.2 mM ($n = 6$). This suggests that the $K_{\text{d(low-aff.choline)}}$ for the effect of choline on fluorescence changes is due to choline binding to the same site that gives rise to choline-induced currents. The 5-fold higher $I_{0.5(\text{choline})}$ value compared with the $K_{\text{d(low-aff.choline)}}$ value is probably due to the following difference. Choline-induced currents reflect total transport, which includes binding of choline to the *cis*-side and choline debinding from the *trans*-side. At variance, the effect of choline on potential-dependent fluorescence changes can be due to binding choline either to the *cis*-side or to the *trans*-side.

Figure 3b shows the effect of various concentrations of TEA on potential-dependent fluorescence changes of TMRM-labeled rOCT1(10ΔC-F483C). Also for TEA, a significantly better fit was obtained if a model for two-site interaction was used for fitting compared with a one-site model. For TEA, a high-affinity site with a $K_{\text{d(high-aff., TEA)}}$ of 57 $\pm$ 10 nM and a low-affinity site with a $K_{\text{d(low-aff., TEA)}}$ of 57 $\pm$ 3 μM was obtained. The latter value is of the same order of magnitude as the $I_{0.5(\text{TEA})}$ value of 240 $\pm$ 31 μM ($n = 4$), which was obtained for activation of TEA-induced currents at -50 mV in oocytes expressing rOCT1(10ΔC-F483C) after 5-min labeling with 100 μM TMRM.

In addition, for the effect of MPP on the potential-dependent fluorescence changes of TMRM-labeled rOCT1(10ΔC-F483C) a biphasic curve was observed, suggesting a high- and a low-affinity interaction site (Fig. 3c). For half-maximal effects at the high-affinity site [$K_{\text{d(high-aff., MPP)}}$] and the low-affinity site [$K_{\text{d(low-aff., MPP)}}$] values of 41 $\pm$ 14 pM and 0.87 $\pm$ 0.11 μM were determined, respectively.

Because transported substrates may interact with the outward- and inward-facing conformation of the substrate binding pocket during the transport cycle, it was important to investigate the concentration dependence of a nontransported inhibitor that blocks the turnover. Figure 4 shows the concentration dependence of the effect of TBuA on potential-dependent fluorescence changes. A complex concentration dependence of inhibition curve was obtained. A two-site model yielded a significantly better fit than a one-site model (data not shown); however, a three-site model even revealed a significantly better fit than the two-site model (Fig. 4). For the half-maximal concentrations of TBuA at the three sites, K_d values of 2 $\pm$ 0.7 pM, 0.36 $\pm$ 0.11 nM, and 0.29 $\pm$ 0.07 μM were obtained.

High-Affinity Binding of TBuA Inhibited MPP Uptake. We investigated the effect of cysteine replacement of Phe483 in rOCT1(10ΔC) on the inhibition of MPP uptake by TBuA. rOCT1(10ΔC-F483C) was expressed in oocytes, and uptake of 2.5 nM [^{3}H]MPP—the MPP concentration is 1000 times lower than the K_m for MPP—was determined in the presence of various concentrations of TBuA (Fig. 5a, open squares). An IC$_{50}$ value of 22 $\pm$ 4.5 nM ($n = 5$) was obtained. Approximately the same value (24 $\pm$ 1.3 nM; $n = 2$) was determined in oocytes expressing rOCT1(10ΔC-F483C) that were incubated for 5 min at room temperature with 100 μM
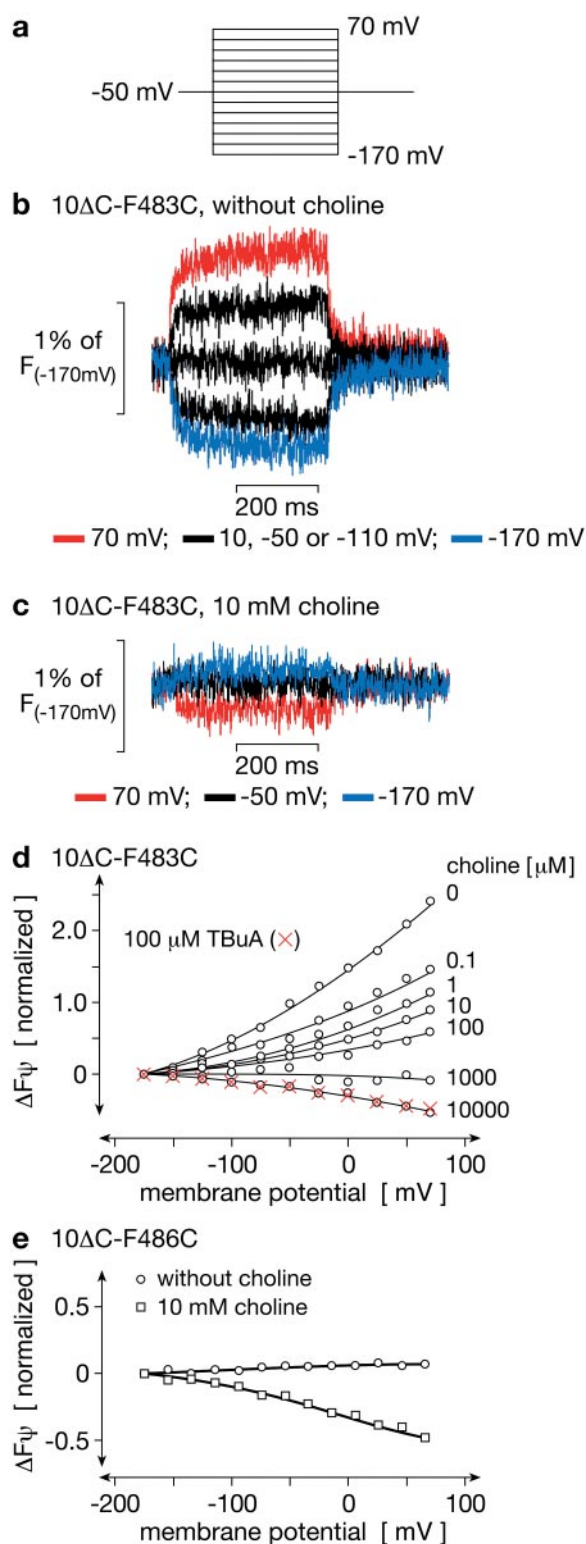
Fig. 2. Voltage- and cation-dependent fluorescence changes in TMRM-labeled mutants rOCT1(10ΔC-F483C) and rOCT1(10ΔC-F486C). Constructs rOCT1(10ΔC-F483C) and rOCT1(10ΔC-F486C) were expressed in oocytes, labeled for 5 min with 5 μM TMRM and washed with Ori buffer. Labeled oocytes were superfused with Ori buffer (b, d, and e), with buffer containing various concentrations of choline (c, d, and e), or with buffer containing 100 μM TBuA (d). a, voltage protocol for membrane potential steps starting from -50 mV. b and c, original traces showing $\Delta F\psi$ of TMRM-labeled rOCT1(10ΔC-F483C) according to the voltage protocol in a. d and e, graphical representation of normalized $\Delta F\psi$ in oocytes expressing rOCT1(10ΔC-F483C) or rOCT1(10ΔC-F486C). $\Delta F\psi$ was normalized as described under *Materials and Methods*. The data indicate potential- and cation-dependent movements of amino acids in positions 483 and 486.

TMRM (Fig. 5a, closed circles). It is noteworthy that values 15 to 20 times higher were obtained with rOCT1(10ΔC) (340 $\pm$ 70 nM; $n = 3$; Fig. 5a) and with wild-type rOCT1 (460 $\pm$ 100 nM; $n = 3$). To determine whether the high-affinity inhibition of rOCT1(10ΔC-F483C) by TBuA is dependent on the substrate used, we also measured the concentration dependence for inhibition of TEA uptake by rOCT1(10ΔC-F483C) compared with rOCT1(10ΔC) and wild-type rOCT1. The measurements were performed with 9 μM [14C]TEA. This concentration is at least 5 times below the K_m values. Thus, competitive interactions at the transport site can be neglected. For TBuA inhibition of TEA uptake, similar IC_{50} values were determined as for TBuA inhibition of MPP uptake [rOCT1(10ΔC-F483C), 11.3 $\pm$ 1.3 nM, $n = 3$; rOCT1(10ΔC), 280 $\pm$ 70 nM, $n = 3$; and wild-type rOCT1, 620 $\pm$ 40 nM, $n = 3$]. These data indicate the binding of TBuA to a high-affinity binding site that does not inhibit cation transport by rOCT1(10ΔC) but leads to a complete inhibition of cation transport by rOCT1(10ΔC-F483C). It is noteworthy that the high affinity for inhibition by TBuA was also observed when rOCT1(10ΔC-F483C) was modified with TMRM.

Why is the affinity obtained for high-affinity TBuA inhibition ($IC_{50} \sim 20$ nM) much lower than that of the high-affinity TBuA sites (site 1, $K_d \sim 2$ pM; site 2, $K_d \sim 0.4$ nM) identified by fluorescence measurements (Fig. 4)? This could be due to allosteric interaction between the high-affinity MPP binding site identified by fluorescence measurements ($K_d \sim 40$ pM; Fig. 3) and the high-affinity TBuA binding sites. Note that TBuA inhibition of MPP uptake was measured with 2.5 nM [3H]MPP, a concentration that saturates the high-affinity MPP site.
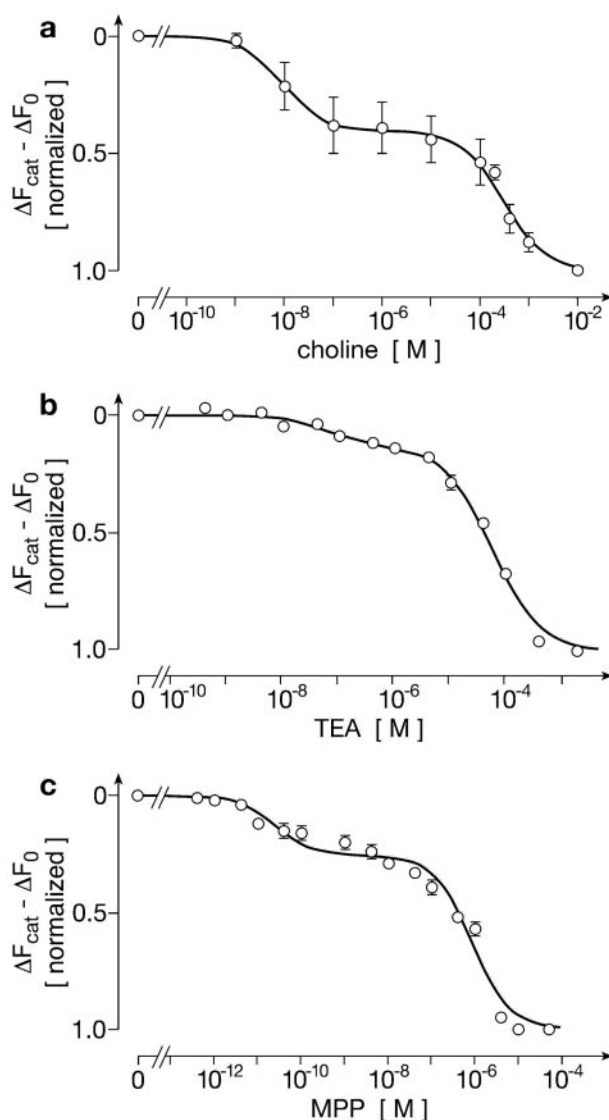
In Fig. 6, we tested whether MPP concentrations in the range of the K_m value for MPP uptake (~ 3 μM; Table 1) compete for high-affinity inhibition of MPP uptake by TBuA in oocytes expressing rOCT1(10ΔC-F483C). The K_m value for MPP uptake is similar to the K_d value of the low-affinity MPP binding site determined by fluorescence measurements (0.87 μM; Fig. 3c) We measured the concentration dependence of TBuA inhibition using MPP concentrations of 2.5 nM, 2 μM, and 40 μM. The obtained IC_{50} values increased with increasing concentrations of MPP. Assuming competitive inhibition and a K_m value for MPP of 3 μM, similar K_i values were calculated from the inhibition curves obtained with the three different substrate concentrations (2.5 nM MPP, 22 $\pm$ 1 nM; 2 μM MPP, 24 $\pm$ 1 nM; 40 μM MPP, 17 $\pm$ 1 nM; $n = 3$ each). These data suggest competition between the high-affinity inhibitory site of TBuA and the low-affinity transport site of MPP.

Detection of Two TBuA Binding Sites by Capacitance Measurements. We have reported online capacitance measurements with oocytes expressing rOCT2 in which the interactions of transported cations and nontransported inhibitors were analyzed (Schmitt and Koepsell, 2005). In the present work, we tested whether more than one TBuA binding site in rOCT1 could be detected by capacitance measurements, too. For this purpose, we expressed rOCT1(10ΔC) or rOCT1(10ΔC-F483C) in oocytes, and we measured the capacitance changes that were induced by various concentrations of TBuA at -50 mV (Fig. 7). When the superfusion solution was switched from Ori buffer to Ori buffer containing 5 nM TBuA, a small but significant capacitance decrease could be observed [(rOCT1-

(10ΔC), −0.11 ± 0.03 nF; and rOCT1(10ΔC-F483C), −0.15 ± 0.04 nF; $n = 4$ each; $P < 0.05$ for difference to capacitance decrease after exchange of Ori buffer]. This indicates a high-affinity TBuA binding site, with a $K_d < 5$ nM. However, the capacitance measurements were not sensitive enough to determine the exact K_d value(s) for this(these) site(s). With both mutants a second TBuA binding site with a K_d value around 1 μM was resolved [rOCT1(10ΔC), 0.95 ± 0.11 μM; and rOCT1(10ΔC-F483C), 1.06 ± 0.37 μM; $n = 4$ for each]. This low-affinity binding site has a similar affinity as the TBuA inhibition site of cation uptake observed in rOCT1 wild type (0.6 μM; Fig. 5) and the low-affinity TBuA binding site detected by fluorescence measurements (0.3 μM; Fig. 4)

A Presumed Interaction between the TMH 11 and TMH 2 Was Critical for Transport. Both observations described above [1) that the exchange of phenylalanine 483 in rOCT1(10ΔC) to cysteine results in high-affinity inhibition of

MPP uptake by TBuA and 2) that low-affinity binding of MPP competes at this inhibitory site with TBuA,] tentatively suggested that phenylalanine or cysteine at position 483 is located close to a TBuA binding site, which is shared with MPP. However, the observation that high-affinity inhibition of cation uptake by TBuA was unaltered when Cys483 was modified by TMRM contradicts this interpretation. In addition, the previously described model structure of rOCT1 with an inward-facing substrate binding pocket suggests that Phe483 is located outside the substrate binding region but forms contact(s) with the TMH 2 (Fig. 8, a and c). Therefore, we considered the possibility that the F483C exchange may disturb the interaction between the TMH 2 and 11 and that binding of TBuA to a high-affinity TBuA binding site in the distant substrate binding region may block a transport-related conformational change in the destabilized rOCT1-(10ΔC-F483C) mutant but not in rOCT1(10ΔC) or in rOCT1
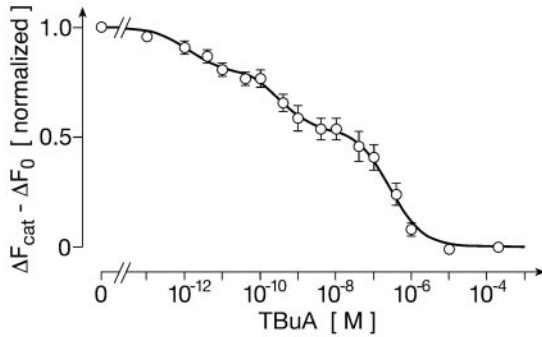

Fig. 3. Potential-dependent fluorescence changes of TMRM-labeled rOCT1(10ΔC-F483C) in the presence of various concentrations of transported substrates. Oocytes expressing rOCT1(10ΔC-F483C) were labeled with 5 μM TMRM. Fluorescence changes as a result of membrane potential changes from +50 to −150 mV were measured in the absence (ΔF_0) and presence of the organic cation substrates (ΔF_{cat}) choline (a), TEA (b), or MPP (c). Substrate-dependent fluorescence changes were normalized as described under *Materials and Methods*. A one-site model and a two-site model were fitted to the data obtained from individual oocytes and to the compiled data sets. The K_d values obtained with the two site-model and the significance levels for the better correlation of the fit with the two-site model compared with the one-site model are presented. The data indicate coexisting high- and low-affinity substrate binding sites.

wild type. To test this hypothesis, we measured TBuA inhibition of MPP uptake after disturbing the postulated interaction between Phe483 and the second TMH by replacing

Fig. 4. Potential-dependent fluorescence changes of TMRM-labeled rOCT1(10ΔC-F483C) in the presence of a nontransported inhibitor. Experiments were performed as in Fig. 3 with the exception that the potential-dependent fluorescence changes were measured in the presence of various concentration of TBuA. A one-site model, a two-site model, and a three-site model were fitted to data from individual oocytes and to the compiled data that are presented in the graph. The K_d values obtained with the three-site model and the significance levels for the better correlation of the fit with the three-site model compared with the two-site model are presented. The data indicate three coexisting binding sites for TBuA.
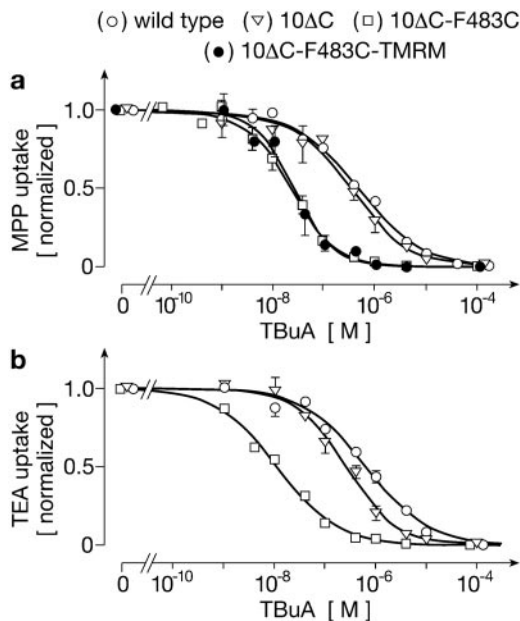

Fig. 5. TBuA-mediated high-affinity inhibition of cation uptake by rOCT1(10ΔC-F483C). Wild-type rOCT1, rOCT1(10ΔC), or rOCT1(10ΔC-F483C) were expressed in oocytes. In one experimental series rOCT1(10ΔC-F483C) was labeled by incubating the oocytes for 5 min with 100 μM TMRM [rOCT1(10ΔC-F483C-TMRM)]. Uptake of 2.5 nM [³H]MPP (a) or 9 μM [¹⁴C]TEA (b) was measured in the presence of various concentrations of TBuA. Mean values ± S.E. of three to five or of two [rOCT1(10ΔC-F483C-TMRM)] individual experiments are shown. The curves were obtained by fitting the Hill equation to the data. The data show that exchange of Phe483 by cysteine leads to high-affinity inhibition of cation uptake by TBuA.

amino acids in the second TMH localized at the presumed contact region (Fig. 8, a and c). Reasoning that the presumed contact region between the TMH 2 and 11 may also include Phe486, we also investigated whether the affinity for TBuA inhibition of MPP uptake is altered in mutant rOCT1(10ΔC-F486C) (Fig. 8, a and c).

After exchange of Asp150 in rOCT1(10ΔC) by cysteine, the affinity for TBuA inhibition of MPP uptake was unchanged (IC$_{50}$ of 0.31 ± 0.09 μM; n = 3). However, when Trp147 was exchanged by cysteine, the affinity for TBuA inhibition of MPP uptake was increased to approximately the same value (IC$_{50}$ of 16 ± 3.5 nM; n = 3 each; Fig. 9a) as in rOCT1(10ΔC-
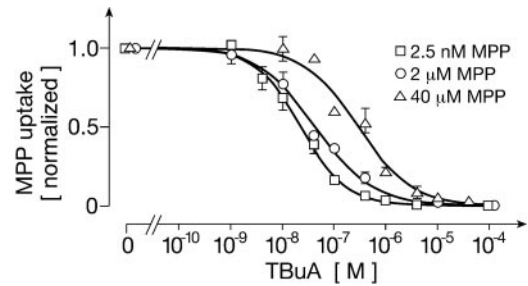

Fig. 6. Competition between the high-affinity TBuA inhibition site and the low-affinity MPP transport site in rOCT1(10ΔC-F483C). rOCT1(10ΔC-F483C) was expressed in oocytes and inhibition of [³H]MPP uptake by TBuA was measured using three different MPP concentrations. Mean values ± S.E. of three independent experiments are shown. The solid lines represent fits of the Hill equation to the data.
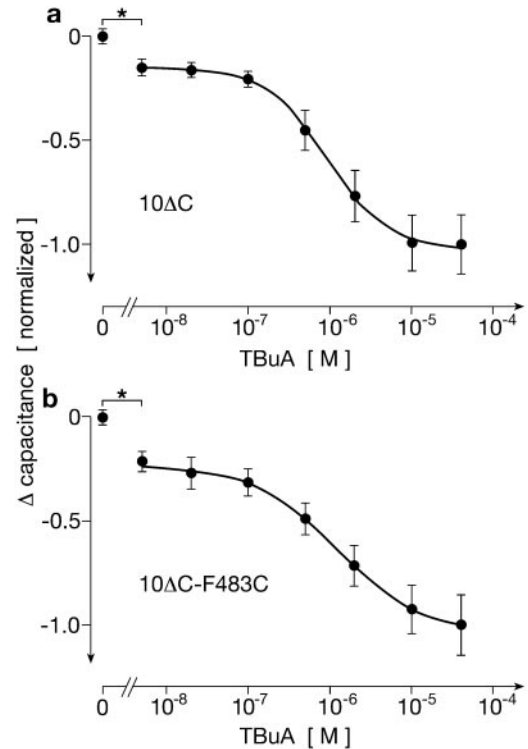

Fig. 7. TBuA-induced capacitance changes. Oocytes expressing rOCT1-(10ΔC) or rOCT1(10ΔC-F483C) were superfused with Ori buffer, clamped to −50 mV, and the effects on capacitance were measured when Ori buffer was exchanged with Ori buffer (zero TBuA concentration) or with Ori buffer containing different concentrations of TBuA. Mean values ± S.E. of four oocytes from two different batches are shown together with the results of fits of the Hill equation to the data (solid lines). The data indicate the existence of a high-affinity ($K_{0.5}$ < 5 nM) and a low-affinity TBuA binding site ($K_{0.5}$ ~ 1 μM) in both mutants. ∗, P < 0.05.

Table (Fig. 4)

| | K_d values [nM] | | | model distinction |
Exp.	site 1	site 2	site 3	3 sites vs. 2 sites
1	0.004	0.66	458	P < 0.01
2	0.001	0.37	132	P < 0.001
3	0.001	0.19	356	P < 0.001
4	0.002	0.24	200	P < 0.01
1–4	0.001	0.32	277	P < 0.001

F483C) (IC$_{50}$ of 22 ± 4.5 nM; n = 5; Fig. 5a). Remarkably, the same affinity for inhibition of MPP uptake by TBuA as in rOCT1(10ΔC-F483C) and rOCT1(10ΔC-W147C) was also obtained when Phe486 was replaced by cysteine (IC$_{50}$ of 23 ± 4.0 nM, n = 3; Fig. 9a). The observation that virtually the same increase in affinity for TBuA inhibition of MPP uptake compared with rOCT1(10ΔC) was obtained when one of three hydrophobic amino acids within the predicted contact area between two TMHs was replaced by cysteine strongly supports our initial hypothesis that interaction between the TMH 2 and 11 is critical for transport.

We also tested how inhibition of MPP uptake by TBuA was influenced when Phe483 was replaced by serine, leucine, or tryptophan (Fig. 9b) or when Trp147 was exchanged by serine. After replacement of Phe483 by serine, a similar IC$_{50}$ value (28 ± 7 nM; n = 3) was obtained for inhibition of MPP uptake by TBuA as after replacement of Phe483 by cysteine, representing a 12-fold affinity increase compared with rOCT1(10ΔC). This suggests that serine and cysteine disturb the hydrophobic interaction between the TMH 2 and 11 in a similar manner. However, after replacement of Phe483 by leucine, the affinity of TBuA to inhibit MPP uptake was only increased 4-fold (IC$_{50}$ = 84 ± 9 nM; n = 3). The inhibition by TBuA remained unchanged when Phe483 was replaced by tryptophan (IC$_{50}$ = 230 ± 60 nM; n = 3). This suggests that a tryptophan in position 483 mediates a sufficiently strong hydrophobic interaction with the second TMH similar to a phenylalanine, whereas leucine is only partially effective. After exchange of Trp147 with serine, an IC$_{50}$ value of 18 ± 1 nM (n = 3) for inhibition of [³H]MPP (2.5 nM) uptake by TBuA was obtained

indicating that serine in this position has a similar effect as cysteine.

We investigated whether the affinity increase of TBuA to inhibit MPP uptake observed after replacement of Phe483 or Trp147 in rOCT1(10ΔC) by serine was also observed when these mutations were introduced into wild-type rOCT1. Figure 10 shows dose-response curves obtained for the inhibition of [³H]MPP (2.5 nM) uptake by TBuA in oocytes expressing wild-type rOCT1, rOCT1(F483S), or rOCT1(W147S). Similar to the observations for rOCT1(10ΔC), both mutations in rOCT1 lead to a significant (P < 0.001) increase in affinity [IC$_{50}$ values: wild-type rOCT1, 460 ± 60 nM; rOCT1(F483S), 19 ± 4 nM; and rOCT1(W147S), 71 ± 9 nM; n = 3 for each]. Although the affinity of rOCT1(W147S) was lower compared with rOCT1(F483S), these data indicate that the affinity increase of TBuA to inhibit MPP uptake observed after mutations of Phe483 or Trp147 in rOCT1(10ΔC) represents intrinsic properties of rOCT1.

A Model of the Outward-Facing Conformation of rOCT1. A structure model of rOCT1 with an outward-facing cleft was obtained by applying a putative rearrangement mechanism to the structure model of the inward-facing conformation of rOCT1 (Popp et al., 2005) as has been proposed for lactose transport of LacY permease (Abramson et al., 2003a,b). The structures of the inward- and outward-facing rOCT1 models (Fig. 8, a and b) can be superimposed, yielding a root-mean-square deviation (r.m.s.d.) of 5.7 Å for all Cα atom positions. If only Cα atoms of residues of the N-terminal domain (first six helices) are used for superposition, the r.m.s.d. is 1.5 Å. Likewise, superimposing residues in the
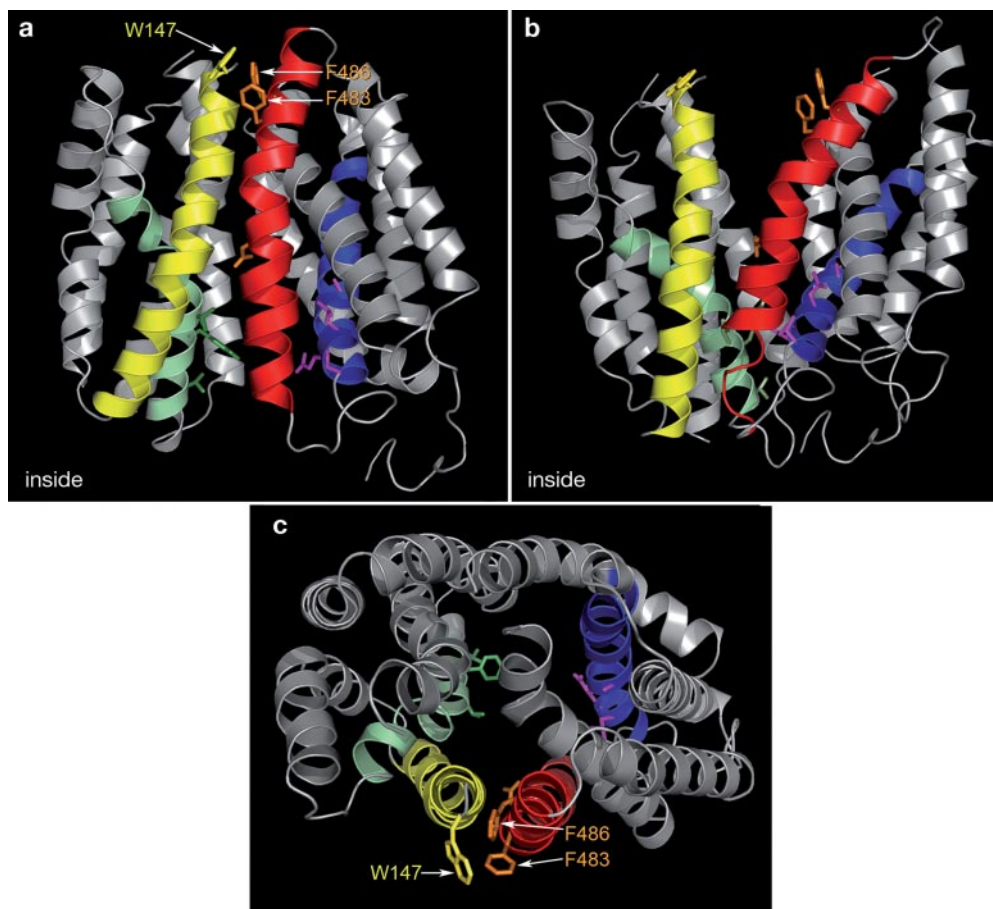

Fig. 8. Models of the inward-facing and the outward-facing conformations of rOCT1. Modeling of the inward-facing conformation shown in a (side view) and c (view from intracellular) has been described previously (Popp et al., 2005), whereas modeling of the outward facing conformation (b) is described under *Materials and Methods*. The TMH 2 is indicated in yellow, the TMH 4 in green, the TMH 10 in blue, and the TMH 11 in red. Amino acids supposed to be directly involved in cation binding within the binding pocket are indicated in ball-and-stick representation without numbering. These are TMH 4: Trp218, Phe222, and Thr226; TMH 11: Asp475; and TMH 10: Ala443, Leu447, Gln448, and Cys451. Amino acids Trp147, Phe483, and Phe486 in the contact area between the TMH 2 and TMH 11 are indicated in ball-and-stick representation with numbering.

C-terminal domain (helices 6–12) yields an r.m.s.d. of 1.7 Å for the Cα positions. These values clearly reflect the rigid-body movement applied to the inward-facing template structure used for modeling. Changes in the packing of the individual helices obtained during energy minimization and in vacuo molecular dynamics simulations explain why the two individual N- and C-terminal parts of rOCT1 domains do not superimpose perfectly. The opening of the inward-facing cleft of the previously described rOCT1 model measures 20 × 10 Å, and the depth of the open pocket formed by helices 1, 2, 4, 5, 7, 8, 10, and 11 reaches approximately two thirds of the helices' length (Fig. 8a). Likewise, the opening on the outward-facing model is roughly 25 × 10 Å, with a pocket depth of roughly 30 Å (Fig. 8b). The models of the two rOCT1 conformations support the proposed movements of amino acids in position 483 and 486. They predict that Phe483 and/or Phe486 in the TMH 11 interact(s) with Trp147 in the TMH 2 in the inward-facing but not in the outward-facing conformation. Both models suggest a transport mechanism by which cations bound to the inner part of the outward-facing cleft are transferred to the other side of the membrane upon rOCT1 switching to the inward-facing conformation.

Discussion

The voltage-clamp fluorometry experiments reported in this study indicate that the phenylalanine residues 483 and 486 of the organic cation transporter rOCT1 take part in conformational changes during the transport cycle. Both phenylalanine residues are located in the TMH 11 close to the extracellular side of the membrane (Fig. 8a). According to the previously reported model structure of rOCT1 with an inward-open binding pocket the phenylalanine residues are oriented toward the lipid phase, and they may interact with Trp147 in the TMH 2 (Fig. 8, a and c). In a model with an outward-open binding pocket, Phe483 and 486 in the TMH 11 are far apart from Trp147 in the TMH 2 (Fig. 8b). This outward-facing model was built using TMH rearrangements that were proposed for LacY permease during sugar transport (Abramson et al., 2003a,b). Our structural models predict large movements in the TMH 2 and 11. However, although 13 amino acid positions in the TMH 11 and Trp147 in the TMH 2 (T. Friedrich and H. Koepsell, unpublished data) were tested for fluorescence changes after introduction and TMRM labeling of cysteines, we detected conformationally sensitive fluorescence changes only in positions 483 and 486. This may have various reasons. For example, TMRM labeling of introduced cysteines may not be possible at all positions due to limited accessibility. Another reason may be that the fluorescence of the bound TMRM responds only to changes in environmental conditions (e.g., whether the dye is shifted from a hydrophobic to a hydrophilic environment or vice versa). Thus, from the absence of fluorescence changes one cannot conclude that TMRM-labeled amino acids do not move during transport and the observed fluorescence changes are not correlated with the degree of spatial movements of the respective cysteines.

The observed potential-dependent conformational shifts of TMRM-labeled Cys483 occurred on a millisecond time scale. They were maximal in the absence of transported cations, indicating a transporter state, which can be switched in a saturating manner between at least two conformational states by voltage jumps. In the presence of transported organic cations, the potential jump-induced fluorescence changes were largely reduced. Under these conditions, the transporter carries out turnover in a concentration-dependent manner. This leads to concentration-dependent redistribution of conformational states within the dynamic equilibrium present under turnover conditions, resulting in accumulation of a transporter state,
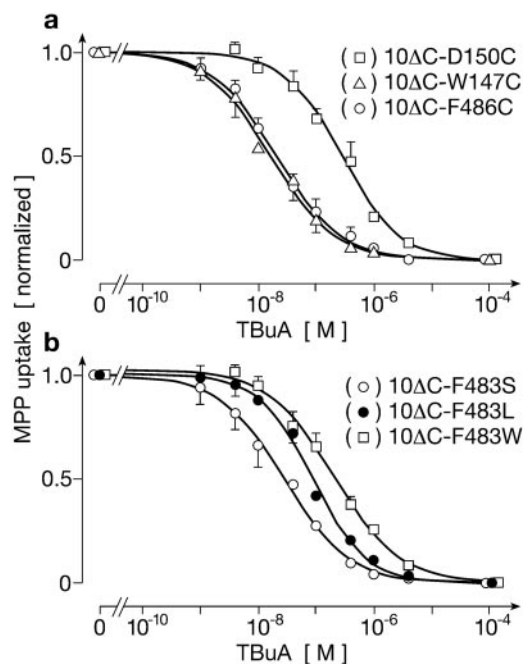

Fig. 9. Inhibition of MPP uptake by TBuA in mutants of rOCT1(10ΔC) with exchanges of amino acids within the predicted contact area between the TMH 2 and TMH 11. Mutants rOCT1(10ΔC-W147C), rOCT1(10ΔC-D150C), and rOCT1(10ΔC-F486C) (a) and mutants rOCT1(10ΔC-F483S), rOCT1(10ΔC-F483L), and rOCT1(10ΔC-F483W) (b) were expressed in oocytes. Uptake of 2.5 nM [³H]MPP was measured in the presence of various concentrations of TBuA. Mean values ± S.E. of three individual experiments are shown. The solid curves were obtained by fitting the Hill equation to the data. These data show that exchange of different amino acids within the predicted contact area between the TMH 2 and 11 leads to high-affinity inhibition of MPP uptake by TBuA, with the same $K_{0.5}$ value (W147C, F483S, F486C, and F483C, see Fig. 5a).
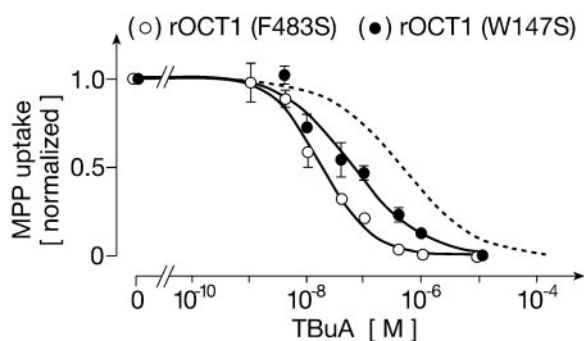

Fig. 10. Inhibition of MPP uptake by TBuA in rOCT1 mutants in which amino acids within the presumed contact area between the TMH 2 and 11 were exchanged. Mutants rOCT1(F483S) and rOCT1(W147S) were expressed in oocytes, and uptake of 2.5 nM [³H]MPP was measured in the presence of different TBuA concentrations. Mean values ± S.E. of three individual experiments are shown, and the Hill equation was fitted to the data. The inhibition curve obtained for wild-type rOCT1 presented in Fig. 5a is indicated for comparison (broken line). The data show that mutations in the predicted contact area between the TMH 2 and 11 of rOCT1 lead to high-affinity inhibition by TBuA similar to that observed for rOCT1(10ΔC).

which cannot be switched by voltage pulses. In presence of the nontransported cation TBuA, the amplitudes of the fluorescence changes that could be evoked by voltage jumps were also reduced. In this case, however, the decrease in fluorescence amplitudes is likely due to binding of TBuA, which may reduce conformational flexibility or may even lock the transporter in a certain conformational state. We exclude that the described organic cation affinities are due to quenching of TMRM by choline, TEA, MPP, and/or TBuA. First, quenching of TMRM by four structurally different organic cations is not supposed to generate high- and low-affinity effects in each case. Second, the potential-dependent fluorescence changes that were decreased by rOCT1 ligands were correlated with transport activity (D. Gorbunov and H. Koepsell, unpublished data).

Using effects of the nontransported cation TBuA on potential-dependent fluorescence changes of TMRM-labeled Cys483 as readout for inhibitor binding, we were able to demonstrate coexistence of three TBuA binding sites in rOCT1. Because TBuA is not transported by rOCT1(10ΔCys), and no permeation of TBuA across the plasma membrane could be detected after 10-min incubation of oocytes with TBuA (C. Volk and H. Koepsell, unpublished data), the different affinities determined for TBuA effects on fluorescence probably represent different interaction sites of TBuA within the outwardly oriented binding pocket. It is noteworthy that the affinity of the three sites is highly different, with K_d values of 2 pM, 0.4 nM, and 0.3 μM. To avoid artifacts by TMRM labeling of endogenous cysteines in rOCT1, we performed the fluorescence measurements by introducing cysteine residues in mutant rOCT1(10ΔC) in which all cysteines, with the exception of those in the large extracellular loop, had been removed. Of course, it cannot be excluded that the affinities for cations were influenced by the mutations in rOCT1(10ΔC-F483C) or by the labeling of Cys483 with TMRM. However, for the following reasons it is highly probable that wild-type rOCT1 contains similar high-affinity binding sites: First, it seems highly improbable that two new high-affinity binding sites for TBuA within the outwardly oriented substrate binding pocket are generated by removal of endogenous cysteine residues and/or replacement of residues with cysteines followed by labeling with TMRM. Specific conservative mutations may increase the affinity of a pre-existing binding site (Gorboulev et al., 2005; Popp et al., 2005); however, multiple mutations are not supposed to form binding sites that do not exist in the wild-type transporter. Second, by inhibition experiments, we detected a high-affinity TBuA binding site with the same affinity in nonlabeled rOCT1(10ΔC-F483C), TMRM-labeled rOCT1(10ΔC-F483C), rOCT1(10ΔC-F483S), rOCT1(10ΔC-W147C), rOCT1(F483S), and rOCT1(W147S). Third, we were also able to demonstrate the existence of a high-affinity TBuA binding site, with a K_d < 5 nM, by capacitance measurements in rOCT1(10ΔC). The existence of a high-affinity MPP binding site of human organic cation transporter OCT1, with a K_d of 6 pM, has been demonstrated by replacement liquid chromatography for the solubilized and immobilized transporter (Moaddel et al., 2005).

Our observations open interesting perspectives concerning the possible reasons for evolutionary development of high-affinity binding sites in rOCT1, their physiological importance, and putative biomedical implications. Polyspecific

transporters that excrete xenobiotics may have been evolved to protect organisms from xenobiotics in the environment. Transporters for endogenous compounds such as choline or monoamine neurotransmitters may have achieved the capability for polyspecific substrate recognition by developing a binding region that contains interaction sites for various compounds. The existence of a polyspecific binding region in organic cation transporters was suggested by single point mutations that lead to affinity changes for individual cations (Gorboulev et al., 1999, 2005; Popp et al., 2005; Zhang et al., 2005), by model analysis of rOCT1 (Popp et al., 2005; Zhang et al., 2005), and by the studies described in the present article. Whereas it can easily be imagined that the substrate binding region of organic cation transporters serves as collector for organic cations with different chemical structures, it is difficult to understand how the binding of cations at various sites may lead to cation translocation. In our attempts to elucidate whether high-affinity cation binding sites may participate in cation transport, we also measured the concentration dependence of [³H]MPP uptake at low MPP concentrations (2.5 to 100 nM MPP in oocytes expressing rOCT1; 1 pM to 100 nM MPP in human embryonic kidney 293 cells, which were stably transfected with rOCT1). Because in these measurements a high-affinity transport site could not be resolved (H. Koepsell, unpublished data), high-affinity cation binding in rOCT1 may not be able to induce translocation. It is possible that translocation is facilitated only when a low-affinity cation binding site is occupied. However, because the translocation probably includes a large conformational change in which a binding pocket containing different binding sites switches between an outward- and inward-facing orientation, cations bound to high-affinity cation binding sites may be translocated together with cations at a low-affinity site. The intracellular release of high-affinity ligands may be facilitated by structural changes within the binding pocket during transition from the outward and inward facing orientation (Volk et al., 2003).

Transport of organic cations may be inhibited in several ways. In addition to competition between two transported cations at the low-affinity transport site, cations bound to low- or high-affinity sites may block the transport mechanism. For example, a bulky cation bound to the low-affinity transport site may not be able to pass a gate-like structure (Schmitt and Koepsell, 2005), or it may directly block the transport mechanism. Another possibility is that binding of a bulky cation to a high-affinity site blocks a transport-relevant conformational change. Such a mechanism may include subtle allosteric structural changes that may cause dramatic effects on transport.

Our study provides an example how destabilization of the tertiary structure of rOCT1 at a model-predicted interaction area between the TMH 2 and 11 allows or alters an allosteric effect after binding of TBuA to a high-affinity site. Whereas TBuA does not induce high-affinity inhibition of MPP or TEA transport by wild-type rOCT1 or rOCT1(10ΔC), cation transport could be blocked already at very low TBuA concentrations if Phe483 or Trp147 at the modeled contact area between the TMH 2 and 11 were replaced by small hydrophilic amino acids. We hypothesize that this contact area is important for the stabilization of the native conformation of rOCT1 because we observed that double mutations in this area (W147S/F483S, W147C/F483C, and W147C/F486C) did not

reach the plasma membrane (D. Gorbunov, V. Gorboulev, and H. Koepsell, unpublished data). The observed functional effects of the single point mutations in the modeled contact area allow several conclusions. First, the predicted interaction between the TMH 2 and 11 is critically involved in transport-related conformational changes of rOCT1. The functional importance of this contact region demonstrated in this work strongly supports the proposed rOCT1 tertiary structure models. Second, destabilizing mutants at transport-relevant interaction points between TMHs may be used to detect and characterize high-affinity cation binding sites by inhibition experiments. Third, instead of changing transport of model cations, a transformation of a high-affinity noninhibitory binding site to a high-affinity inhibition site may occur due to mutations in organic cation transporters. Such mutations can be localized at transport-relevant interaction points between different TMHs or other parts of the transporters that are involved in transport-relevant structural changes. Thus, small concentrations of cationic drugs in the body that do not change the function of wild-type transporters may block transport in patients carrying such mutations in OCT transporters.

In summary, we showed that OCT1 contains high-affinity cation sites in addition to low-affinity transport sites. We raise the hypothesis that organic cations bound to high-affinity sites can be translocated together with organic cations at low-affinity sites. Cation binding to high-affinity sites may not disturb low-affinity cation transport in wild-type OCT1. However, mutations of amino acids in transport-relevant key positions, which can be distinct from the cation binding region, may transform noninhibitory high-affinity binding sites to high-affinity inhibition sites and thereby give way to adverse drug reactions in patients.

References

Abramson J, Smirnova I, Kasho V, Verner G, Iwata S, and Kaback HR (2003a) The lactose permease of *Escherichia coli*: overall structure, the sugar-binding site and the alternating access model for transport. *FEBS Lett* **555**:96–101.

Abramson J, Smirnova I, Kasho V, Verner G, Kaback HR, and Iwata S (2003b) Structure and mechanism of the lactose permease of *Escherichia coli*. *Science* **301**:610–615.

Arndt P, Volk C, Gorboulev V, Budiman T, Popp C, Ulzheimer-Teuber I, Akhoundova A, Koppatz S, Bamberg E, Nagel G, et al. (2001) Interaction of cations, anions, and weak base quinine with rat renal cation transporter rOCT2 compared with rOCT1. *Am J Physiol Renal Physiol* **281**:F454–F468.

Budiman T, Bamberg E, Koepsell H, and Nagel G (2000) Mechanism of electrogenic cation transport by the cloned organic cation transporter 2 from rat. *J Biol Chem* **275**:29413–29420.

Busch AE, Quester S, Ulzheimer JC, Waldegger S, Gorboulev V, Arndt P, Lang F, and Koepsell H (1996) Electrogenic properties and substrate specificity of the polyspecific rat cation transporter rOCT1. *J Biol Chem* **271**:32599–32604.

Geibel S, Kaplan JH, Bamberg E, and Friedrich T (2003) Conformational dynamics of the Na$^+$/K$^+$-ATPase probed by voltage clamp fluorometry. *Proc Natl Acad Sci U S A* **100**:964–969.

Gorboulev V, Shatskaya N, Volk C, and Koepsell H (2005) Subtype-specific affinity for corticosterone of rat organic cation transporters rOCT1 and rOCT2 depends on three amino acids within the substrate binding region. *Mol Pharmacol* **67**:1612–1619.

Gorboulev V, Volk C, Arndt P, Akhoundova A, and Koepsell H (1999) Selectivity of the polyspecific cation transporter rOCT1 is changed by mutation of aspartate 475 to glutamate. *Mol Pharmacol* **56**:1254–1261.

Gründemann D, Gorboulev V, Gambaryan S, Veyhl M, and Koepsell H (1994) Drug excretion mediated by a new prototype of polyspecific transporter. *Nature* **372**: 549–552.

Gründemann D and Koepsell H (1994) Ethidium bromide staining during denaturation with glyoxal for sensitive detection of RNA in agarose gel electrophoresis. *Anal Biochem* **216**:459–461.

Ho SN, Hunt HD, Horton RM, Pullen JK, and Pease LR (1989) Site-directed mutagenesis by overlap extension using the polymerase chain reaction. *Gene* **77**: 51–59.

Koepsell H and Endou H (2004) The SLC22 drug transporter family. *Pflugers Arch* **447**:666–676.

Koepsell H, Lips K, and Volk C (2007) Polyspecific organic cation transporters: structure, function, physiological roles, and biopharmaceutical implications. *Pharm Res* **24**:1227–1251.

Koepsell H, Schmitt BM, and Gorboulev V (2003) Organic cation transporters. *Rev Physiol Biochem Pharmacol* **150**:36–90.

Moaddel R, Yamaguchi R, Ho PC, Patel S, Hsu C-P, Subrahmanyam V, and Wainer IW (2005) Development and characterization of an immobilized human organic cation transporter based liquid chromatographic stationary phase. *J Chromatogr B Analyt Technol Biomed Life Sci* **818**:263–268.

Nezu J-I, Tamai I, Oku A, Ohashi R, Yabuuchi H, Hashimoto N, Nikaido H, Sai Y, Koizumi A, Shoji Y, et al. (1999) Primary systemic carnitine deficiency is caused by mutations in a gene encoding sodium ion-dependent carnitine transporter. *Nat Genet* **21**:91–94.

Palmieri O, Latiano A, Valvano R, D'Incà R, Vecchi M, Sturniolo GC, Saibeni S, Peyvandi F, Bossa F, Zagaria C, et al. (2006) Variants of OCTN1–2 cation transporter genes are associated with both Crohn's disease and ulcerative colitis. *Aliment Pharmacol Ther* **23**:497–506.

Pao SS, Paulsen IT, and Saier MH Jr (1998) Major facilitator superfamily. *Microbiol Mol Biol Rev* **62**:1–34.

Peltekova VD, Wintle RF, Rubin LA, Amos CI, Huang Q, Gu X, Newman B, Van Oene M, Cescon D, Greenberg G, et al. (2004) Functional variants of OCTN cation transporter genes are associated with Crohn disease. *Nat Genet* **36**:471–475.

Popp C, Gorboulev V, Müller TD, Gorbunov D, Shatskaya N, and Koepsell H (2005) Amino acids critical for substrate affinity of rat organic cation transporter 1 line the substrate binding region in a model derived from the tertiary structure of lactose permease. *Mol Pharmacol* **67**:1600–1611.

Reitman ML and Schadt EE (2007) Pharmacogenetics of metformin response: a step in the path toward personalized medicine. *J Clin Invest* **117**:1226–1229.

Schmitt BM and Koepsell H (2002) An improved method for real-time monitoring of membrane capacitance in *Xenopus laevis* oocytes. *Biophys J* **82**:1345–1357.

Schmitt BM and Koepsell H (2005) Alkali cation binding and permeation in the rat organic cation transporter rOCT2. *J Biol Chem* **280**:24481–24490.

Sturm A, Gorboulev V, Gorbunov D, Keller T, Volk C, Schmitt BM, Schlachtbauer P, Ciarimboli G, and Koepsell H (2007) Identification of cysteines in rat organic cation transporters rOCT1 (C322,C451) and rOCT2 (C451) critical for transport activity and substrate affinity. *Am J Physiol Renal Physiol* **293**:F767–F779.

Tokuhiro S, Yamada R, Chang X, Suzuki A, Kochi Y, Sawada T, Suzuki M, Nagasaki M, Ohtsuki M, Ono M, et al. (2003) An intronic SNP in a RUNX1 binding site of *SLC22A4*, encoding an organic cation transporter, is associated with rheumatoid arthritis. *Nat Genet* **35**:341–348.

Veyhl M, Spangenberg J, Püschel B, Poppe R, Dekel C, Fritzsch G, Haase W, and Koepsell H (1993) Cloning of a membrane-associated protein which modifies activity and properties of the Na$^+$-D-glucose cotransporter. *J Biol Chem* **268**:25041–25053.

Volk C, Gorboulev V, Budiman T, Nagel G, and Koepsell H (2003) Different affinities of inhibitors to the outwardly and inwardly directed substrate binding site of organic cation transporter 2. *Mol Pharmacol* **64**:1037–1047.

Wang Y, Meadows TA, and Longo N (2000) Abnormal sodium stimulation of carnitine transport in primary carnitine deficiency. *J Biol Chem* **275**:20782–20786.

Wang Y, Ye J, Ganapathy V, and Longo N (1999) Mutations in the organic cation/carnitine transporter OCTN2 in primary carnitine deficiency. *Proc Natl Acad Sci U S A* **96**:2356–2360.

Zhang X, Shirahatti NV, Mahadevan D, and Wright SH (2005) A conserved glutamate residue in transmembrane helix 10 influences substrate specificity of rabbit OCT2 (SLC22A2). *J Biol Chem* **280**:34813–34822.

Address correspondence to: Dr. Hermann Koepsell, Institute of Anatomy and Cell Biology, Koellikerstr. 6, 97070 Würzburg, Germany. E-mail: hermann@koepsell.de